UVA and UVB elicit distinct mutational signatures in melanoma

Rebecca C. Hennessey[1] *, Robert L. Bowman[5] *, David A. Tallman[1,2], Tirzah J. Weiss[1,2], Emma R. Crawford[2], Brandon M. Murphy[1], Amy Webb[3], Souhui Zhang[1], Krista M. D. La Perle[4], Craig J. Burd[2], Ross L. Levine[5], A. Hunter Shain[6] and Christin E. Burd[1,2†]

[1]Departments of Cancer Biology and Genetics, [2] Molecular Genetics, [3]Biomedical Informatics, and [4]Veterinary Biosciences, The Ohio State University, Columbus, Ohio, 43210
[5]Human Oncology and Pathogenesis Program, Memorial Sloan Kettering Cancer Center, New York, NY 10065
[6]Departments of Dermatology and Pathology, Helen Diller Family Comprehensive Cancer Center, University of California, San Francisco (UCSF), San Francisco, CA 94115

* Authors contributed equally

RUNNING TITLE
UVA and UVB signatures in murine melanoma

KEY WORDS
mouse model, uveal melanoma, ultraviolet (UV) radiation, NRAS, BRAF

ADDITIONAL INFORMATION
Financial support: This work was supported by the Melanoma Research Alliance (309669 to C.E.B.), Damon Runyon Foundation (38-16 to C.E.B and 22-17 to R.L.B.), Pelotonia (R.C.H., E.R.C.) and The National Institutes of Health (F31CA236418 to B.M.M. and P30 CA016058 to The Ohio State University Comprehensive Cancer Center).

†Address correspondence to:
Christin E. Burd
The Ohio State University
Biomedical Research Tower, Rm 918
460 W. 12th Avenue
Columbus, Ohio 43210, USA
Phone: (614)688-7569
Fax: (614)292-6356
Email: burd.25@osu.edu

Conflict of interest statement: R.L.L. is on the supervisory board of Qiagen, is a scientific advisor to Imago, C4 Therapeutics and Isoplexis which include equity interest. He is a former SAB member of Loxo which was acquired by Eli Lilly. He receives research support from and consulted for Celgene and Roche and has consulted for Lilly, Janssen, Astellas, Morphosys and Novartis. He has received honoraria from Roche, Lilly and Amgen for invited lectures and from Gilead for grant reviews.

Article metrics:
Word count (main text): 4,478 words
7 Figures
0 Tables
6 Supplemental Figures/Tables

ABSTRACT

It is difficult to discern the relative contributions of ultraviolet-A (UVA; 320-400nm) and ultraviolet-B (UVB; 280-320nm) radiation to human melanoma development. Here, we compared the tumorigenic consequences of a single UVA or UVB exposure in mouse models predisposed to Braf- or Nras-mutant melanoma. Exposures approximated the amount of UVA or UVB energy contained in ~40 minutes of summer sunlight. While UVA accelerated melanoma onset in a subset of mice, UVB universally reduced tumor latency and induced gene mutations relevant to the human disease. Genomic analyses uncovered distinct mutational signatures specific to each UV spectrum. The UVB-specific signature was biased for mutations on the untranscribed DNA strand and closely mirrored mutational signatures enriched in human cutaneous melanoma. The UVA-specific signature mimicked SBS51, a mutational signature found in human uveal melanoma. Distinctions in the trinucleotide patterns of the UVA and UVB signatures suggest that cytosine deamination plays a key role in UVB-mediated melanomagenesis.

INTRODUCTION

Genomic and epidemiological data suggest that ultraviolet radiation (UV) is the major etiologic agent in melanoma. Two UV spectra reach Earth's surface: UVA (320-400 nm) and UVB (280-320 nm) [1]. UVA is the most prevalent form of UV in terrestrial sunlight; however, it is poorly absorbed by DNA [1-4]. By contrast, UVB can directly damage DNA and is the major form of UV responsible for erythema [4]. The mutational effects of UV irradiation are apparent in human melanoma genomes, which exhibit one of the highest somatic mutation rates of any tumor type [5,6]. UV has also been linked to melanoma risk through epidemiological studies showing increased incidence in individuals with a history of childhood sunburns, tanning bed use, or intense, intermittent UV exposures [7]. While these observations establish correlative relationships between UV irradiation and melanoma formation, there is limited understanding of the genetic events and relative risk conveyed by different UV spectra.

Genetically engineered mouse models (GEMMs) provide a controlled genetic background in which the genomic and phenotypic effects of specific UV exposures can be studied. It is known that neonatal or chronic UV treatment accelerates the formation and progression of melanoma in a variety of GEMMs [8-12]. Tumors from several UV-treated GEMMs have been sequenced, including those representative of the most common genetic subtypes of melanoma: NRAS- and BRAF-mutant [8,12,13]. However, the only study that has sequenced both UVA- and UVB-induced tumors used a chronic UV dosing scheme and was unable to identify any mutational patterns specific to each spectrum [8].

Here, we used a single-dose UV irradiation scheme to characterize the phenotypic and genomic effects of UVA and UVB exposure in Nras- and Braf-mutant mouse models. We exposed these animals to a single dose of UVA or UVB, approximating the amount of energy from each UV spectrum in 40 minutes of intense sunlight. Then, we monitored the mice for melanoma development. Tumors from these animals were sequenced to gain insight into the genomic mechanisms by which each UV spectrum influences melanoma formation.

RESULTS

UV exposure alters Nras- and Braf-mutant melanomagenesis

We generated *TN* and *TB* mice to model the major genetic subtypes of human melanoma [14] (**Figure 1A, B**). *TN* mice are homozygous for the *LSL-Nras*^{Q61R} allele [10,15], whereas *TB* animals carry a heterozygous, conditional *Braf*^{V637E} allele (*Braf*^{CA} [16]). Oncogene expression is driven by the endogenous gene promoter in both models, and is activated by a melanocyte-specific, tamoxifen-inducible Cre recombinase (*Tyr::CreER(T2)* [17]). Therefore, the expression of oncogenic Nras or Braf in these mice mimics the presence of *NRAS* and *BRAF* mutations in most benign human nevi [18]. Mice carrying only the *Braf*^{CA} allele rarely develop melanoma [19]. Therefore, *p16*^{INK4a} conditional knockout alleles (*p16*^{L}, [20]) were included in both the *TN* and *TB* models. While p16^{INK4a} loss-of-function is an early event observed in >60% of human melanomas, germline mutations affecting p16^{INK4a} are insufficient to drive the disease in mice or humans [10,21,22].

TN and *TB* mice were treated with 4-hydroxytamoxifen (4OHT) on postnatal days one and two to induce Cre activity and stimulate recombination of the conditional *p16*^{INK4a} knockout and *LSL-Nras*^{61R} or *Braf*^{CA} alleles. On postnatal day three, the mice were exposed to a single dose of ambient light ("No UV"), UVA or UVB irradiation. The amount of UVB delivered approximated that which is contained in 40 minutes of summer sunlight (4.5 kJ/m^2; see: **Methods**), whereas the amount of UVA employed models a short, indoor tanning session (70 or 150 kJ/m^2; see: **Methods**). These dosing schemes approximate sun exposures of a similar duration, as the UVB to UVA ratio in sunlight is ~1:20, but varies based on season, cloud cover and latitude [23].

The onset of spontaneous melanoma was compared among mice exposed to No UV, UVA or UVB irradiation. Exposure to a single dose of 4.5 kJ/m^2 UVB did not cause erythema or blistering, but dramatically accelerated melanoma onset and decreased overall survival in both the *TN* and *TB* models (**Figures 1C-D** and **Suppl. Figure S1**). Exposure to 70 kJ/m^2 UVA also enhanced melanoma formation, but with greatly reduced penetrance (**Figure 1C-D**). Doubling this dose of UVA in the *TN* model did not further facilitate melanoma formation, suggesting that 70 kJ/m^2 UVA was sufficient to elicit the maximal response achievable with a single treatment (**Figure 1C**). Together, these results reveal the potent ability of UVB to stimulate melanoma formation in *TN* and *TB* mice. Furthermore, our findings suggest that UVA can facilitate melanoma onset in some settings, albeit to a much lesser extent than UVB.

We next examined the incidence and growth phenotypes of tumors arising in each of our experimental cohorts. Tumor incidence increased in UVB-exposed *TN* mice, but was not significantly altered in *TN* animals treated with UVA or *TB* mice exposed to any form of UV (**Figure**

1E). Tumor distribution and burden were also similar between male and female *TN* and *TB* mice regardless of exposure, with ~59% of tumors arising on the trunk, ~13% on the head and ~16% on the ears or tail (**data not shown**). Once established, *TN* and *TB* tumors grew at the same rate regardless of exposure (**Figure 1F**). Therefore, enhanced tumorigenesis, rather than more rapid melanoma growth, is responsible for the reduction in overall survival observed in UVB-exposed *TN* and *TB* mice.

We postulated that melanomas arising in UVA- or UVB-exposed mice would exhibit distinct histopathological features. Therefore, we examined hematoxylin and eosin stained tumor sections representative of the rate of onset and body site distribution of melanomas from each cohort. Tumors from both models contained variable percentages of myxoid and spindle cells with comparable degrees of invasion, mitosis and granulocyte infiltration regardless of treatment (**Suppl. Figure S2A-C**, **data not shown**). A paucity of pilosebaceous units and hyperplasia of the overlying epidermis was also observed in UVA, UVB and unexposed mice of both genotypes (**Suppl. Figure S2A&F**). Most tumors from the UVB-treated *TN* cohort contained neoplastic cells with plasmacytoid features that were not prevalent in *TN* melanomas from the UVA and No UV cohorts (6 of 7 vs. 2 of 6 and 0 of 5 tumors, respectively; **Suppl. Figure S2D**). Fibroblastic features were seen in UVA-treated *TN* melanomas (3 of 6), but were not overtly apparent in tumors from other *TN* mice (**Suppl. Figure S2E**). Unlike the *TN* model, tumor samples from *TB* mice contained areas of pigmentation, typically characterized by multiple clusters of melanophages distributed at the dermal-hypodermal interface with or without associated neoplastic cells and occasionally within the tumors (**Suppl. Figure S2F**). These results show that although the histopathological features of cutaneous murine and human melanomas differ, a single UVA or UVB exposure can promote the formation of cutaneous, murine tumors with distinct morphologic features.

UVB exposure humanizes the genome of *TN* and *TB* melanomas

In contrast to human melanomas, GEMM-derived tumors are frequently characterized by a high burden of genomic copy number alterations (CNAs) and few single nucleotide variants (SNVs) [6,14,24-26]. Thus, we used whole exome sequencing (WES) to determine whether a single UVA or UVB exposure would promote the formation of murine melanomas with 'humanized' cancer genomes containing a high frequency of SNVs. The burden of CNAs was reduced in all *TN* tumors exposed to UVB and in 5 of 7 *TN* tumors exposed to UVA (**Figure 2A, B**). Conversely, neonatal UV treatment had little effect on the number of CNAs detected in *TB*-derived melanomas (**Figure 2A, B**). The most commonly observed CNA in *TB* tumors was a gain in chromosome 6,

the region in which *Braf* resides (**Figure 2A**). Consistent with this observation, 5 of 12 *TB* melanomas showed increased Braf protein expression as compared to normal, murine skin (**Figure S3**). Recurring copy number gains in chromosomes 1 and 10 were also observed in tumors from the *TB*-UVA, *TN*-No UV and *TN*-UVA groups (**Figure 2A**).

To determine the SNV burden of tumors from our UVA- and UVB-treated GEMMs, we aligned each melanoma genome to the mm10 reference genome, removed variants observed in pooled normal controls, and excluded polymorphisms observed in dbSNP [27]. The average SNV burden of melanomas from both *TN* and *TB* mice increased as a result of prior UVB exposure, whereas the SNV burden of UVA-irradiated *TN* and *TB* tumors was slightly higher, but not statistically different, than that observed in tumors from the No UV groups (**Figure 2C**). The frequency of insertion and deletions (indels) did not differ in tumors from irradiated and unirradiated *TB* mice, but increased slightly in *TN* UVB melanomas as compared to unirradiated controls (**Figure 2D**).

WES also revealed UV-dependent changes in the specific gene ontologies mutated in *TN* and *TB* melanomas. In both models, more of the SNVs and indels discovered in the UVB groups overlaped with genes frequently altered in human melanoma than SNVs and indels identified in the No UV tumors (**Suppl. Figure S4**). Overlapping genes included those encoding protein products involved in cell adhesion (cadherins, demoplakin), vesicular trafficking (dyneins, myosins, actin remodeling enzymes), the extracellular matrix (collagens, laminins), epigenetic gene regulation (*Brd1*, *Chd8*, *Kdm2c*, *Kmt2c*, *Kmd2d*), and receptor tyrosine kinase signaling (*Erbb4*, *Igfr*, *Mtor*, *Pten*) (**Suppl. Figure S4**). In contrast to published sequencing studies of melanomas broad-spectrum or UVB-irradiated GEMMs [8,12,13], *Trp53* mutations were extremely rare in our cohort (1 in 36 tumors).

We next used Ingenuity Pathway Analysis (IPA) to identify mutated gene ontologies enriched in tumors from each of our experimental cohorts. Genes mutated in *TN* and *TB* tumors from the No UV and UVA cohorts were rarely linked to melanoma, whereas the top five disease and biological functions altered in melanomas derived from UVB-exposed *TN* and *TB* mice included “cutaneous melanoma”, “melanoma”, “skin cancer”, and “skin tumor” (**Figure 2E**, **Suppl. Table 1**). Together, these data establish that a single dose of UVB induces a high burden of disease-relevant SNVs in *TN* and *TB* tumors.

C>T transitions are the predominant mutation type driven by UVA and UVB

The elevated frequency of cytosine to thymidine (C>T) transitions in human melanoma is often attributed to UVA and UVB irradiation [28]. To test whether UV-treatment enriched for C>T transitions in our GEMMs, we quantified the burden of each SNV type (C>A, C>G, C>T, T>A,

T>C or T>G) in melanomas from *TN* and *TB* mice treated with No UV, UVA or UVB. As anticipated, melanomas from UVA- and UVB-treated *TN* and *TB* mice had a greater number of C>T transitions than unirradiated controls (**Figure 3A** and **Suppl. Table 2A**; $p < 0.043$ for each group vs. No UV). Since methylated cytosines form cyclobutane pyrimidine dimers (CPDs) with higher efficiency [29], we separately analyzed C>T alterations occurring within a CpG site. We found that the majority of C>T alterations occurred within non-CpG sites, suggesting that methylated cytosines may not be preferentially mutated in our models (**Figure 3A**). UVB also increased the total number of T>C (A>G) and T>A mutations in *TB* tumors ($p < 0.032$ for both groups vs. No UV); however, these mutation types were not similarly elevated in melanomas from UVB-irradiated *TN* mice (**Suppl. Table 2A**).

We further evaluated the mutation type data, accounting for variances in tumor mutational load by determining the contribution of individual SNV types to the total mutational burden of each experimental group. Consistent with our analysis of mutational burden, C>T transitions at non-CpG sites were enriched in tumors from both UVA- and UVB-treated models as compared to No UV controls (**Figure 3B** and **Suppl. Table 2B**; $p < 0.045$ for all UV-No UV pairs). This enrichment of C>T mutations was accompanied by global decreases in the frequency of most other SNV types. An exception to this observation was the enrichment of T>A transversions in melanomas from UVA-treated *TN* mice ($p < 0.007$ for UVA vs. No UV). T>A transversions were also more frequent in melanomas from UVA-irradiated *TB* mice, but this enrichment did not reach statistical significance ($p < 0.16$ for UVA vs. No UV).

We looked for evidence of oncogene-dependent mutational enrichments and found that C>T transitions were both more abundant ($p < 0.05$) and frequent ($p < 8.20\text{x}10^{-5}$) in *TB*-UVB tumors than *TN*-UVB tumors (**Figure 3**, **Suppl. Table 2A-B**). Other mutation types did not differ significantly in number or frequency between the two genotypes. Together, our findings highlight the dominance of C>T transitions in melanomas from both UVA- and UVB-treated mice and suggest that an underlying *Braf* mutation may promote further accumulation of these mutations. Furthermore, we provide evidence that UVA irradiation may drive the acquisition of both C>T transitions and T>A transversions.

UVA and UVB drive C>T mutations in distinct trinucleotide contexts

CPD-associated C>T lesions are considered classical 'UVB signature mutations' and occur preferentially at dipyrimidine sites [30]. C>T transitions in other, non-cutaneous cancers lack this specificity [31]. We used lego plots to visualize the trinucleotide context of C>T mutations in tumors from our *TN* and *TB* models (**Figure 4A**). Most C>T transitions occurred at dipyrimidine sites in

UVA- and UVB-induced melanomas from both models (**Figure 4B-C**, red bars). However, UVB-associated C>T transitions were enriched in TCG and CCA sites, whereas UVA-associated C>T mutations were more evenly distributed amongst the eight potential dipyrimide triplets (**Figure 4B-C**, back two rows of red bars).

The enrichment of T>A transversions in our UVA-induced tumors (**Figure 3** and **Suppl. Table 2A-B**) led us to investigate the preferred trinucleotide context of these mutations. The majority of UVA-induced T>A transversions followed a 5' thymidine residue and, remarkably, the same nucleotide preference was observed for C>A transversions in these tumors (**Figure 4B-C**). These data highlight the preferential mutation of pyrimidines with a 5'T in melanomas from UVA-treated *TN* and *TB* mice. Furthermore, our results show that UVA and UVB promote C>T mutations with distinct trinucleotide contexts.

UVB-induced mutations localize to the non-transcribed strand

Studies in cultured fibroblasts and model organisms implicate transcription-coupled repair (TCR) in the rapid resolution of UV-induced DNA lesions [32]. Therefore, we investigated whether the SNVs observed in our *TN* and *TB* tumors exhibited a strand bias. C>T and T>C mutations were biased towards the untranscribed strand in all tumors regardless of exposure or model (**Figure 5**, **Suppl. Table 2C**). By contrast, C>A transitions were enriched on the transcribed strand, and the remaining mutation types (C>G, T>A, T>C) showed variable strand bias, dependent on the experimental group (**Figure 5**). All mutation types were enriched on the untranscribed strand in tumors from UVB-treated *TB* mice, and *TN* UVB tumors showed a similar shift in strand enrichment compared to unirradiated controls (**Figure 5**). These data support a role for TCR in the resolution of both UV-induced and naturally occurring C>T and T>C mutations. Our results also show that unlike UVA, UVB promotes the accumulation of a variety of SNV types on the untranscribed DNA strand.

Identification of distinct UVA and UVB mutational signatures

Non-negative matrix factorization was used to identify the three most prevalent signatures in our complete dataset: Signatures A, B and C (**Figure 6A**). Signature A was enriched in UVB tumors from both models as compared to melanomas from mock and UVA irradiated mice of the same genotype ($p < 0.01$ for all comparisons; **Figure 6B**, **Suppl. Table 2D**). Signature B was lower in *TN* UVA tumors than in *TN* No UV or UVB melanomas ($p < 0.002$ for both comparisons), but did not change in *TB* tumors facilitated by different forms of UV (**Figure 6B**, **Suppl. Table 2D**). Interestingly, Signature C was enriched in *TN* UVA ($p < 1.0\text{x}10^{-8}$) and *TB* UVA ($p < 0.006$)

tumors as compared to melanomas from No UV and UVB mice of the same genotype (**Figure 6B**, **Suppl. Table 2D**). Thus, Signature A appears to define melanomas from UVB-treated *TN* and *TB* mice, whereas Signature C is specifically linked to tumors arising after UVA exposure.

Mutational signatures enriched in human skin cancer are biased towards the untranscribed DNA strand [30]. A similar strand bias was seen in our UVB signature, Signature A, whereas our UVA-associated signature, Signature C, exhibited variable strand bias (**Figure 6C**). These data are consistent with the idea that transcription coupled repair (TCR) plays a larger role in the resolution of DNA lesions induced by UVB than UVA.

Murine UVA and UVB signatures mimic distinct COSMIC mutational signatures

The COSMIC mutational signature most closely associated with human skin cancers and melanoma prognosis is Signature 7, which has recently been divided into four sub-signatures: SBS7a-d (See: [8,33]). Interestingly, Signature A in our dataset had a high degree of similarity with SBS7a and SBS7b (cosine of similarity = 0.83, $p < 6.98\text{x}10^{-48}$; cosine of similarity = 0.86, $p < 6.06\text{x}10^{-55}$, respectively), however, Signatures C best aligned with SBS50, SBS51 and SBS58 (**Figure 7A**; cosine of similarity = 0.68, $p < 8.00\text{x}10^{-19}$; cosine of similarity = 0.61, $p < 1.23\text{x}10^{-14}$; cosine of similarity = 0.66, $p < 1.23\text{x}10^{-17}$ respectively). The etiology of SBS50, SBS51 and SBS58 is unknown [33].

We next performed the converse analysis, looking to see if any COSMIC signatures were enriched in our murine melanoma datasets. While SBS7a contributed equally to the mutational patterns of No UV, UVA and UVB tumors, SBS7b was significantly enriched in *TN* UVB and *TB* UVB melanomas (**Figure 7B**, **Suppl. Table 2E**). Other signatures increased in tumors from both UVB-accelerated models included: SBS2 which may be linked to APOBEC deamination, SBS10b, which is associated with hypermutated samples, and SBS19 which is of unknown etiology. SBS2 was also enriched in UVA-induced tumors, however, SBS51 showed the highest specificity for our *TN* UVA and *TB* UVA samples.

Because only UVA can pass through the cornea [34], we hypothesized that both SBS51 and our UVA-associated Signature C would be enriched in a subset of uveal melanomas. Compared to acute myeloid leukemia (AML) and cutaneous melanoma (CM), a greater percentage of uveal melanoma samples within the TCGA dataset exhibited the SBS51 signature (**Figure 7C;** $p < 0.041$ and $p < 3.3\text{x}10^{-5}$ respectively). Signature C was similarly enriched in the same uveal melanoma samples as compared to CM, but no difference was seen between UVM and AML samples (**Figure 7D;** UVM vs AML $p < 0.45$; UVM vs CM $p < 6.6\text{x}10^{-11}$). These data support a potential role for UVA in the formation of a subset of uveal melanomas.

DISCUSSION

Human melanoma has one of the highest mutational burdens of any tumor type [30]. Yet, tumors arising in most melanoma GEMMs, including our unirradiated *TN* and *TB* mice, are largely characterized by CNAs rather than SNVs [6,14,24-26]. Here we find that a single UVB exposure can resolve this conundrum and effectively recapitulate the high burden of SNVs in human melanoma. Moreover, tumors from UVB-irradiated *TN* and *TB* mice are enriched for somatic alterations and mutational signatures characteristic of human melanoma (**Figs. 2E, 6B**). These data are consistent with genomic analyses in other UVB-accelerated GEMMs and support the use of irradiated models in pre-clinical melanoma research [8,12,13]. Our results indicate a disparity in the melanomagenic potential of UVA and UVB. Along with prior publications [8,35], these data provide additional evidence that UVA exposures can increase melanoma risk, but not to the same extent as UVB. What distinguishes this study from past investigations is that we have used our GEMMs to identify and characterize distinct mutational signatures arising as a consequence of each UV type. These signatures provide critical insights into the differences between UVA and UVB carcinogenesis.

As might be expected, C>T transitions are the prevailing mutation type in melanomas from *TN* and *TB* mice treated with either UVA or UVB (**Fig. 3**). This observation corroborates previous conclusions that dipyrimidine photoproducts are the major lesions involved in both UVA- and UVB-dependent melanocyte carcinogenesis. HPLC-MS/MS data from human skin and primary keratinocyte cultures estimate the CPD yield from UVB to be 10^3-10^5 fold greater per $J \cdot m^{-2}$ than UVA [36]. Thus, we expected our UVB dose of 4.5 kJ/m^2 to induce at least 240 times more dipyrimidine photoproducts than our UVA dose of 70 kJ/m^2. However, we find that the total number of C>T mutations in tumors from our UVA- and UVB-irradiated *TN* and *TB* GEMMs differs by only 2- and 7-fold, respectively (**Fig. 3A**). There are several possible explanations for this observation which are not mutually exclusive. First, UVA penetrates deeper into the skin than UVB and may reach melanocytes within the hair follicle and dermis with higher efficiency [1]. Alternatively, the majority of melanocytes may die as a consequence of UVB, but not UVA irradiation. Several reports support this model showing that melanocytes are extremely resistant to UVA-mediated cell death [37-39]. Interestingly, we were unable to detect TUNEL positive melanocytes in our models following 4.5 kJ/m^2 of UVB irradiation (data not shown), making this mechanism unlikely. Different rates of photoproduct repair could also explain the lower than expected ratio of UVB:UVA-induced C>T mutations in our GEMMs. UVA has been implicated in the oxidation of a number of nucleotide excision repair (NER) components, including RPA, PCNA, XPA, XPE and XPA [1]. A reduction in the activity of one or several of these components may

compromise photoproduct repair in UVA-irradiated cells and explain why UVA-induced CPDs take longer to resolve [36]. UVB damage also causes keratinocytes to produce paracrine factors like α-Melanocyte Stimulating Hormone (αMSH) and Endothelin-1 (End-1), which activate ataxia telangiectasia mutated (ATM) and ataxia telangiectasia and Rad3-related (ATR), resulting in a DNA damage response which could enhance the recognition and repair of UV photolesions [40]. Thus, *in vivo* CPD repair rates may be faster and more efficient in UVB- versus UVA-irradiated melanocytes. Finally, differences in the types of dipyrimidine photoproducts induced by each UV source could explain why UVB is less mutagenic than predicted. For example, TT CPDs, which are reportedly the least mutagenic dipyrimidine dimer, appear to make up 90% of CPDs in UVA-irradiated DNA, but only 54% of CPDs in UVB-irradiated DNA [23]. Determining the relative role of each of these processes in UVB carcinogenesis will require further investigations using tissue-specific knockouts and rapid melanocyte isolation protocols.

Our observation that TCG triplet-associated C>T mutations are enriched in tumors from *TN* and *TB* mice irradiated with UVB, but not UVA (**Fig. 4B-C**), provides insight into how UVB drives melanocyte carcinogenesis. Experimental models employing the *lacZ* transgene as a mutagenic reporter show that TCG-associated C>T mutations are more prevalent when mice are irradiated with longer UV wavelengths [41]. Therefore, we expected C>T mutations embedded in a TCG triplet to be more frequent in our UVA-irradiated models. This was not the case (**Fig. 4B-C**). TCG sites are known hotspots for UV-mutagenesis for several reasons. UVA and UVB induce TC dimers at twice the frequency of CC or CT dimers [23,42]. Once dimerized, cytosines within a CPD lesion appear to deaminate a million-times faster than those contained in undamaged dsDNA [43]. This process is further enhanced by a catalysis reaction involving the carbonyl group of a 3' guanine residue [43]. Deamination of cytosine to uracil and ^{m}C to thymidine results in TU and TT dimers, which cause a C>T transition upon repair by the bypass DNA polymerase, Pol η [44]. Because the $t_{1/2}$ of TCG-associated CPDs seems to be in the range of several hours [45], the longer these lesions go unresolved, the more likely that deamination will occur. These observations have led us to consider the possibility that differences in the frequency of TCG-associated T>C mutations among UVA and UVB tumors reflect the prolonged chemical or physical persistence of CPDs in UVB-irradiated melanocytes from our models. Persistence could be due to a number of UVB-specific challenges, including: 1) a higher initial burden of lesions, 2) altered melanocyte proliferation, and 3) differences in the types of CPDs elicited. It is interesting to note when *pol η* is deleted from murine cells, C>T transitions decrease in TCG triplets and become enriched within CCA sites [46]. This suggests that the CCA bias observed in our UVB-irradiated tumors could result from the use of other translesion synthesis enzymes.

Efforts to parse the mutational signatures of UVA and UVB have been hindered by a lack of data in which melanoma onset can be attributed to a single form of UV irradiation. However, exploiting the controlled genetic background and tunable UV sensitivity of our models, we were able to derive distinct mutational signatures induced by UVA (Signature C) or UVB (Signature A) (**Fig. 6A-B**). Signature A is enriched in human cutaneous melanomas and exhibits high concordance with COSMIC mutational signatures associated with UV damage (SBS7a, SBS7b; **Fig. 7A, D**). Signature C, however, aligns closely with human mutational signatures of unknown origin (SBS51, SBS53; **Fig. 7A**). Increased frequencies of C>A and T>A transversions distinguish our UVA-enriched Signature C from Signature A (**Figs. 4B-C**, **6A-B**). While C>A transversions likely result as a consequence of UVA-induced guanine oxidation, the origin of T>A mutations is unclear. Of note, >90% of $BRAF^{V600E}$ mutations are caused by T>A transversions, suggesting a possible role for UVA in the etiology of these alterations [47].

The potential enrichment of Signature C in human uveal melanomas is interesting, as UVA has superior tissue penetrance and is more likely than UVB to reach melanocytes within the eye [34]. Unfortunately, there is no available uveal melanoma dataset large enough to separate tumors of the choroid from those of the iris and ciliary body to which UVA can penetrate [34]. The fact that uveal melanomas lack conical UV mutation signatures (e.g. SBS7a/b; **Figure 7b**) has led to speculation that UV irradiation may play a minor role in this disease [48]. However, welders, who are occupationally exposed to full-spectrum UV irradiation, are at increased risk for uveal melanoma [49]. Whether this risk could be due to UVA is unclear. Using polysulphone dosimeters it is estimated that shielded welders still experience up to 90-150 kJ/m^2 of facial UV irradiation in an 8 hour day [50,51]. However, polysulphone dosimeters do not measure UVA, which can penetrate materials like glass. Therefore, UVA exposures are likely to be high and should be further explored as an occupational hazard in welders.

Mutations in Signature A and SBS7a/b are biased to the untranscribed DNA strand. This bias has been attributed to differences in the efficiency of transcription-coupled repair (TCR) as compared to global genome repair (GG-NER). TCR rapidly recruits NER components to UV-induced DNA lesions within actively transcribed genes, whereas GG-NER is responsible for resolving mutations throughout the genome [52]. Why our UVA-enriched mutational signatures, SBS51, SBS53 and Signature C, exhibit inconsistent transcriptional strand bias is unclear (**Fig. 6C**). It is similarly possible that the damage response, burden and types of lesions induced by each form of UV underlie this observation.

Together, our data suggest a model in which C>T transitions are at the crux of both UVA- and UVB-mediated carcinogenesis. The limited frequency of TCG-associated C>T mutations in

melanomas from UVA- versus UVB-irradiated mice, supports a model in which melanocyte carcinogenesis and melanoma formation is associated with the persistence of CPDs after irradiation. Since the melanoma onset is more dramatically impacted by UVB than UVA, methods to enhance the rate of CPD resolution should mitigate the ability of sunlight to facilitate skin cancer formation.

MATERIALS AND METHODS

Mouse models

All animal research protocols were reviewed and approved by The Ohio State University Institutional Animal Care and Use Committee (Protocol #2012A00000134). The *TN* and *TB* models employ a tamoxifen-inducible transgenic allele (*Tyr::CreER(T2)*) to drive melanocyte-specific CRE recombinase activity [17]. In these models, the endogenous *Nras* or *Braf* and *Cdkn2a* loci are modified such that CRE activation leads to the production of mutant $Nras^{Q61R}$ [15] or $Braf^{V637E}$ (equivalent to human $BRAF^{V600E}$) [16] and loss of $p16^{INK4a}$ expression [20] (**Figure 1A, B**). All mice were backcrossed >7 generations to pigmented, C57Bl/6J mice.

Cre induction and UV exposure

Inducible knock-in and knockout alleles were activated with 20 mM 4-hydroxytamoxifen on post-natal (p.n.) days one and two as described [15]. Subjects from each litter were randomly assigned to receive either ambient light (No UV), UVA or UVB on p.n. day three. Mice are unfurred at three days of age. Therefore, the use of a depilatory agent was unnecessary. UVB was delivered to the dorsal side of each animal as a single dose of 4.5 kJ/m^2 using a fixed position, 16W, 312nm UVB light source (Spectronics #EB-280C). [See [10] for additional source information.] UVA was similarly delivered using a 16W source containing two BLE-8T365 bulbs (Spectronics). Based upon the spectrum of these bulbs, the calculated McKinlay-Diffey erythemal effective energy (EEE) of the original 70 kJ/m^2 dose is 14.2 mJ/cm^2 [53]. The average tanning parlor dose is 4.5 Standard Erythema Doses (SEDs; [54]). One SED is equivalent to 10 mJ/cm^2 EEE-weighted UV light [53]. Therefore, an individual receives >3 times more UVA in an average tanning session than a mouse in our 70 kJ/m^2 experimental protocol (45 mJ/cm^2 / 14.2 mJ/cm^2 = 3.17).

Outcome monitoring and histopathology

Mice were randomly numbered following treatment and blindly monitored three times a week for tumor formation. Established melanomas were measured by calipers at least three times per week and tumor size (width × length (mm)) recorded until protocol exclusion criteria were met. Representative tumors were harvested from each cohort, fixed in 10% neutral buffered formalin, routinely processed and embedded in paraffin wax. Sections (4 µm) were stained with hematoxylin and eosin (H&E), and evaluated by a veterinary pathologist, certified by the American College of Veterinary Pathologists (KMDL), using an Olympus BX45 light microscope with attached DP25 digital camera (B&B Microscopes Limited, Pittsburgh, PA). Tumor morphology was assessed as described by Banerjee and Harris [55]. In each sample the extent of skin and subcutis tumor invasion, tumor pigmentation and the maximum number of mitotic figures were

determined from three different fields of view using a 40x objective and 10x ocular lens with a field number of 22 mm.

Sample preparation and whole exome sequencing

Tumor DNA was isolated from flash frozen tissue using the Quick-DNA Miniprep Plus Kit (Zymo Research). Tissues were placed in 2 mL tubes containing 190 µL of diluted Zymo Solid Tissue Buffer and 3.0 mm zirconium beads (Sigma Aldrich Cat# Z763902). Samples were then subjected to homogenization using the Precellys Evolution Homogenizer (Bertin Instruments) using the preset elastic setting: speed: 6,800 RPM, cycle: 4 X 30 sec, pause: 45 sec. Homogenized samples were then incubated in 20 mg/mL of Proteinase K overnight at 55°C before continuing with the Solid Tissues protocol as described for the Quick-DNA Miniprep Plus Kit. Control DNA was generated from toe clips or splenic tissue derived from ten representative *TN* and ten representative *TB* animals. These controls were then combined at an equal ratio and concentrated using the Genomic DNA Clean & Concentrator-10 kit (Zymo Research).

The integrity and concentration of resulting genomic DNA was confirmed on an Aglient TapeStation and Life Technologies Qubit. Indexed libraries were generated from 200 ng of genomic DNA using the Kapa Hyper Prep and Agilent SureSelectXT Mouse All Exon target enrichment systems. Exome hybridization was conducted using 500 ng of each DNA library and the resulting target-enriched fragments PCR-amplified (11 cycles). Indexed libraries were pooled and subjected to paired-end 150 bp sequencing on an Illumina HiSeq4000. Average target coverage was 75X (range 53 - 107X). Raw data files were deposited in the NCBI Sequence Read Archive (SRA) under accession #PRJNA574176.

Sequence Alignment, Processing and Variant Calling

Sequences were aligned to mm10 using BWA (version 0.7.15) [56]. Duplicates were removed using Picard (version 2.17.11) [57] and the resulting sequences re-aligned around indels (GATK version 3.6) [58]. Tumor variants (SNVs and indels) were called from unambiguously mapped reads using VarScan2 (version 2.4) [59] and annotated using Variant Effect Predictor from Ensembl [60]. Variants found in pooled normal controls (uninvolved skin from *TB* and *TN* mice) or listed in NCBI dbSNP build 150 were excluded.

Analysis of SNVs and CNAs

SNV burden (variants per Mb) was calculated as a function of the total capture region. Discovered SNVs mapping to murine genes with an identified human ortholog were used to determine the mutational overlap between mouse and human tumors. Genes altered in ≥15% of

human tumors were identified using provisional TCGA data [61]. Oncoprints were made with ComplexHeatmap version 2.0.0 [62] and enriched gene ontologies identified using Ingenuity Pathway Analysis (QIAGEN Inc.) [63]. To calculate the overlap with human tumors, CNAs were identified using CNVkit [64]. Reported CNAs passed a $\log_2$ segmentation threshold of 0.2 with support from at least five bins. Genome fraction containing a CNA was determined by computing the footprint of segments surpassing the copy number threshold and dividing this by the total footprint of all segments.

Mutational spectrum analysis

The total burden and relative contribution of each mutation type to No UV-, UVA- and UVB-induced melanomas was determined using the "mut_type occurences" algorithm in the R package for *MutationalPatterns* [65]. Differences in the absolute number of mutations were assessed using a Mann-Whitney U test. Differences in frequency of each SNV type between UVA or UVB samples versus controls (No UV) were determined using t-tests with Holm's adjustment for multiple comparisons ($p < 0.05$ considered significant).

Lego plots were generated in Matlab after SNVs in each tumor were classified into one of the 96 possible trinucleotide context substitutions (6 substitution classes X 4 possible flanking 5' bases X 4 possible flanking 3' bases), averaged across samples from the same experimental group, and normalized to the relative rate at which each respective trinucleotide repeat occurs within the mm10 exome.

MutationalPatterns was used to examine strand bias, identify *de novo* mutational signatures and compare mutational signatures with those appearing in COSMIC version 3 [33]. *De novo* signatures were selected using non-negative matrix factorization, and a rank of 3 was selected based on maximization of variance explained and a cophenetic score. To assess the enrichment of our *de novo* or COSMIC v3 signatures, we used a modified version of the "fit_to_signatures" function in the *MutationalPatterns* package that allowed for the evaluation of strand sensitive mutational signatures. COSMIC v3 signatures were attained from Alexandrov et al. [33]. Patients were binned into the signature-present group if the contribution of a given signature was non-zero. We used a Fischer Exact Test to determine if the proportion of patients showing the presence or absence of a signature was significantly different between disease groups.

Immunoblotting

Flash-frozen tumors were homogenized in PBS with Halt phosphatase inhibitor (Thermo Scientific) and protease inhibitor (Sigma) using the Precellys Evolution Homogenizer with Cryolys

(Bertin Instruments). The preset elastic setting was used for homogenizing. Tumor homogenates were centrifuged to remove PBS and resuspended in RIPA buffer with phosphatase and protease inhibitors. Lysates were sonicated 2 x 10 seconds using a Branson digital sonifier at 10% amplitude. Samples were centrifuged at 15,000 rpm for 5 min at 4°C and supernatants collected and quantified by Bradford assay (BioRad). Samples (35 µg total) were blotted for BRAF (Santa Cruz sc-5284; 1:500) and β-Actin (Cell Signaling #3700; 1:1000) and imaged using a LI-COR Odyssey CLx system. Bands were quantified using Image Studio Version 5.2 software (LI-COR Biosciences).

FIGURE LEGENDS

Figure 1. Neonatal UV exposure alters melanoma initiation in *TN* and *TB* mice. A, *TN* mice are homozygous for a melanocyte-specific, tamoxifen-inducible CRE transgene (*Tyr::CreER(T2)*), a conditional $p16^{INK4a}$ knockout allele ($p16^{L}$), and a conditional $Nras^{Q61R}$ knock-in allele (*LSL-*$Nras^{Q61R}$). Open triangles represent Lox P sites. A star indicates the location of the *Nras* Q61R mutation. **B,** *TB* mice carry a single, $Braf^{V637E}$ conditional allele (*LSL-*$Braf^{CA}$) and are homozygous for *Tyr::CreER(T2)* and $p16^{L}$. Note that $BRaf^{V637E}$ is the murine equivalent of human $BRAF^{V600E}$. Open triangles represent Lox P sites and the location of the V637E mutation is indicated by a star. **C & D,** Kaplan-Meier curves depicting the melanoma-free survival of *TN* (C) and *TB* (D) mice treated on postnatal day three with a single dose of ambient light (No UV), UVA or UVB. Statistical significance was determined by comparing values from control (0 kJ/m^2) and UV-irradiated animals of the same genotype using Gehan-Breslow-Wilcoxon tests. † = $p < 0.0001$, ** = $p < 0.01$. **E,** Total tumor burden of control and UV-irradiated *TN* and *TB* mice at euthanasia. Each circle represents a single mouse. Boxes represent the mean and interquartile range for each group. Whiskers span from the minimum to the maximum value. Statistical significance was determined using two-tailed, unpaired t-tests with Welch's correction. ** = $p < 0.01$ vs. control (0 kJ/m^2) animals of the same genotype. **F,** Average tumor growth rates for UVB- and mock-exposed *TN* and *TB* mice. Each circle represents a single tumor (*TN*: 0 kJ/m^2 n=17; 70 kJ/m^2 UVA n=21; 150 kJ/m^2 UVA n=21; 4.5 kJ/m^2 UVB n=41; *TB*: 0 kJ/m^2 n=27; 70 kJ/m^2 UVA n=10; 4.5 kJ/m^2, n=41). Data are presented as described in E.

Figure 2. UV alters the genomic landscape of *TN* and *TB* tumors. A, Heatmap showing areas of genomic gain or loss within each sequenced tumor. Columns correspond to individual tumors and rows correspond to genomic bins. **B,** Fraction of each sequenced melanoma genome exhibiting a CNA is graphed as a box plot with whiskers set at the 5th and 95th percentiles. Dots represent individual tumors. p-values determined by ANOVA with Dunn's correction. **C-D,** SNVs (C) and indels (D) per megabase of captured genome are plotted and analyzed as in 'B'. **E**, Relative enrichments of the indicated IPA disease functions in mutations from each tumor group. For **A-D**, * = $p < 0.05$, ** $p<0.01$, *** = $p < 0.001$.

Figure 3. C>T mutations predominate in both UVA- and UVB-induced melanomas. A-B, Absolute mutation burden (A) and frequency (B) of each mutation type in *TN* and *TB* tumors arising after mock (No UV), UVA or UVB exposure. Note that C>T transitions are broken into two

classes: those that occur within CpG sites (light red) and those that do not (dark red). See **Suppl. Table 2A-B** for a complete listing of p-values for all comparisons.

Figure 4. UVA- and UVB-induced C>T transitions occur within different tri-nucleotide contexts. A, Diagram showing the layout of trinucleotide mutations in each lego plot. The mutated base is indicated by the color of the bar. The location of the bar within the 4 x 4 color block grid is indicative of the nucleotide sequence surrounding each mutation. The height of each bar corresponds to the average number of mutations in the indicated experimental group, normalized to the relative frequency of the relevant trinucleotide sequence in the mouse exome. **B-C,** Lego plots showing the average frequency of mutations within each trinucleotide context for the indicated experimental cohorts. Total frequencies of each mutation type are shown in the associated pie charts.

Figure 5. UVA and UVB drive tumor-associated mutations with distinct strand bias. The strand location of each mutation type was determined from aggregate data from the indicated mouse models and exposures. Plotted are the log-transformed ratios of transcribed versus untranscribed mutations. Statistical significance of strand bias was assessed using a Poisson test, where an * indicates significant enrichment. Complete p-value listings can be found in **Supplemental Table 2C**.

Figure 6. Enrichment of disease-relevant mutational signatures in UVB-induced *TN* and *TB* tumors. A, Non-negative matrix factorization (NMF) was used to identify *de novo* mutational signatures in sequenced *TN* and *TB* melanomas. Three signatures were selected based on explained variance and cophenetic score. The relative contribution of each mutation type and trinucleotide context is shown for each signature. Mutations occurring on the transcribed strand are indicated by open bars, whereas mutations occurring on the untranscribed strand are depicted as closed bars. **B,** Enrichment of identified signatures in tumors from each model and exposure type. Significant differences between groups were assessed using student's t-tests with Holm-Bonferroni correction. Complete p-value listings appear in **Supplemental Table 2D**. **C,** Strand bias of the indicated mutation types within each *de novo* signature shown in (A). p-values were generated using a Poisson test as in **Figure 5**. * = $p < 0.05$

Figure 7. Differential enrichment of COSMIC mutational signatures in UVA- and UVB-induced *TN* and *TB* tumors. A, Heatmap depicting the cosine similarity score between *de novo* signatures discovered in our dataset and COSMIC signatures derived from human tumors. **B,** Shown is the relevant enrichment of each COSMIC mutational signature in *TN* and *TB* tumors from mice exposed to No UV (pink), UVA (green), or UVB (blue). Complete p-value listings appear in **Supplemental Table 2E**. **C,** Shown in blue is the proportion of acute myeloid leukemia (AML, n = 121), cutaneous melanoma (CM, n = 466) and uveal melanoma (UVM, n = 79) samples in the TCGA database that contain the indicated COSMIC mutational signature. **D,** The proportion of AML, CM and UVM samples from (B) that contain the indicated mutational signature, shown in Figure 6A and derived from the *TN* and *TB* mouse models.

SUPPLEMENTAL FIGURE LEGENDS

Figure S1. Overall survival of *TN* and *TB* mice treated with No UV, UVA or UVB. A&B, Kaplan-Meier curves depicting the overall survival rates of *TN* and *TB* mice treated on postnatal day three with a single dose of ambient light (No UV), UVA or UVB. Mice were euthanized after meeting pre-determined exclusion criteria due to tumor burden or malaise. Statistical significance was determined by comparing values from control (0 kJ/m^2) and UV-treated animals of the same genotype using Gehan-Breslow-Wilcoxon tests. † = $p < 0.0001$, ** = $p < 0.01$

Figure S2. Representative photomicrographs of cutaneous tumors from *TN* and *TB* mice. A, *TN* and *TB* tumors, regardless of UV exposure history, contain variable proportions of spindle (left, cellular) and myxoid (right, spaces) morphologies. Bar = 200 µm. **B&C,** Higher magnification images of the myxoid ('B', bar = 20 µm) and spindle ('C', bar = 20 µm) morphologies depicted in 'A'. Arrows = mitotic figures. **D,** Representative image of the neoplastic cells with plasmacytoid features seen in the majority of *TN* tumors evaluated. (circles; bar = 20 µm). **E,** Half of the tumors in UVA-treated *TN* mice exhibited a fibroblastic phenotype with abundant collagen (indicated by *; bar = 20 µm). **F,** Tumor samples from *TB* mice contained areas of pigmentation, typically appearing as clusters of melanophages at the dermal-hypodermal interface (boxes, bar = 200 µm). All images are of H&E stained tissues.

Figure S3. Characterization of Braf levels in *TB* tumors. A, Immunoblot of Braf and β-Actin expression in representative *TB* tumors. **B,** Quantification of the immunoblot shown in 'A'.

Figure S4. Oncoprint of mutated genes relevant to human melanoma in *TN* and *TB* tumors. Shown are genes that were mutated in at least one murine tumor sample and altered at a frequency of 15% or more in the TCGA human melanoma provisional dataset.

REFERENCES

1. Khan, A.Q., Travers, J.B. & Kemp, M.G. Roles of UVA radiation and DNA damage responses in melanoma pathogenesis. *Environ Mol Mutagen* **59**, 438-460 (2018).
2. Pfeifer, G.P., You, Y.H. & Besaratinia, A. Mutations induced by ultraviolet light. *Mutat Res* **571**, 19-31 (2005).
3. Sutherland, J.C. & Griffin, K.P. Absorption spectrum of DNA for wavelengths greater than 300 nm. *Radiat Res* **86**, 399-409 (1981).
4. Setlow, R.B. The wavelengths in sunlight effective in producing skin cancer: a theoretical analysis. *Proc Natl Acad Sci U S A* **71**, 3363-3366 (1974).
5. Bailey, M.H.*, et al.* Comprehensive Characterization of Cancer Driver Genes and Mutations. *Cell* **173**, 371-385 e318 (2018).
6. Zhang, T., Dutton-Regester, K., Brown, K.M. & Hayward, N.K. The genomic landscape of cutaneous melanoma. *Pigment Cell Melanoma Res* **29**, 266-283 (2016).
7. Lo, J.A. & Fisher, D.E. The melanoma revolution: from UV carcinogenesis to a new era in therapeutics. *Science* **346**, 945-949 (2014).
8. Trucco, L.D.*, et al.* Ultraviolet radiation-induced DNA damage is prognostic for outcome in melanoma. *Nat Med* **25**, 221-224 (2019).
9. Chagani, S.*, et al.* Ablation of epidermal RXRalpha in cooperation with activated CDK4 and oncogenic NRAS generates spontaneous and acute neonatal UVB induced malignant metastatic melanomas. *BMC Cancer* **17**, 736 (2017).
10. Hennessey, R.C.*, et al.* Ultraviolet radiation accelerates NRas-mutant melanomagenesis: A cooperative effect blocked by sunscreen. *Pigment Cell Melanoma Res* **30**, 477-487 (2017).
11. Perez-Guijarro, E., Day, C.P., Merlino, G. & Zaidi, M.R. Genetically engineered mouse models of melanoma. *Cancer* **123**, 2089-2103 (2017).
12. Mukhopadhyay, P., Ferguson, B., Muller, H.K., Handoko, H.Y. & Walker, G.J. Murine melanomas accelerated by a single UVR exposure carry photoproduct footprints but lack UV signature C>T mutations in critical genes. *Oncogene* **35**, 3342-3350 (2016).
13. Viros, A.*, et al.* Ultraviolet radiation accelerates BRAF-driven melanomagenesis by targeting TP53. *Nature* **511**, 478-482 (2014).
14. Hodis, E.*, et al.* A landscape of driver mutations in melanoma. *Cell* **150**, 251-263 (2012).
15. Burd, C.E.*, et al.* Mutation-specific RAS oncogenicity explains NRAS codon 61 selection in melanoma. *Cancer discovery* **4**, 1418-1429 (2014).
16. Dankort, D.*, et al.* A new mouse model to explore the initiation, progression, and therapy of BRAFV600E-induced lung tumors. *Genes & development* **21**, 379-384 (2007).
17. Bosenberg, M.*, et al.* Characterization of melanocyte-specific inducible Cre recombinase transgenic mice. *Genesis* **44**, 262-267 (2006).
18. Roh, M.R., Eliades, P., Gupta, S. & Tsao, H. Genetics of melanocytic nevi. *Pigment Cell Melanoma Res* **28**, 661-672 (2015).
19. Dankort, D.*, et al.* Braf(V600E) cooperates with Pten loss to induce metastatic melanoma. *Nat Genet* **41**, 544-552 (2009).
20. Monahan, K.B.*, et al.* Somatic p16(INK4a) loss accelerates melanomagenesis. *Oncogene* **29**, 5809-5817 (2010).
21. Shain, A.H.*, et al.* The Genetic Evolution of Melanoma from Precursor Lesions. *N Engl J Med* **373**, 1926-1936 (2015).
22. Bishop, J.A.*, et al.* Genotype/phenotype and penetrance studies in melanoma families with germline CDKN2A mutations. *J Invest Dermatol* **114**, 28-33 (2000).

23. Cadet, J. & Douki, T. Formation of UV-induced DNA damage contributing to skin cancer development. *Photochem Photobiol Sci* **17**, 1816-1841 (2018).
24. Zloza, A.*, et al.* Workshop on challenges, insights, and future directions for mouse and humanized models in cancer immunology and immunotherapy: a report from the associated programs of the 2016 annual meeting for the Society for Immunotherapy of cancer. *J Immunother Cancer* **5**, 77 (2017).
25. Wang, J.*, et al.* UV-induced somatic mutations elicit a functional T cell response in the YUMMER1.7 mouse melanoma model. *Pigment Cell Melanoma Res* **30**, 428-435 (2017).
26. Krauthammer, M.*, et al.* Exome sequencing identifies recurrent somatic RAC1 mutations in melanoma. *Nat Genet* **44**, 1006-1014 (2012).
27. Kitts, A., Phan, L., Ward, M.H. & Holmes, J.B. The Database of Short Genetic Variation (dbSNP). in *The NCBI Handbook* (National Center for Biotechnology Information, Bethesda (MD), 2013).
28. Cadet, J. & Wagner, J.R. DNA base damage by reactive oxygen species, oxidizing agents, and UV radiation. *Cold Spring Harb Perspect Biol* **5**(2013).
29. Tommasi, S., Denissenko, M.F. & Pfeifer, G.P. Sunlight induces pyrimidine dimers preferentially at 5-methylcytosine bases. *Cancer Res* **57**, 4727-4730 (1997).
30. Alexandrov, L.B.*, et al.* Signatures of mutational processes in human cancer. *Nature* **500**, 415-421 (2013).
31. Mitchell, D.L., Jen, J. & Cleaver, J.E. Sequence specificity of cyclobutane pyrimidine dimers in DNA treated with solar (ultraviolet B) radiation. *Nucleic Acids Res* **20**, 225-229 (1992).
32. Marteijn, J.A., Lans, H., Vermeulen, W. & Hoeijmakers, J.H. Understanding nucleotide excision repair and its roles in cancer and ageing. *Nat Rev Mol Cell Biol* **15**, 465-481 (2014).
33. Alexandrov, L.B.*, et al.* The Repertoire of Mutational Signatures in Human Cancer *bioRxiv* (2018).
34. Yam, J.C. & Kwok, A.K. Ultraviolet light and ocular diseases. *Int Ophthalmol* **34**, 383-400 (2014).
35. Noonan, F.P.*, et al.* Melanoma induction by ultraviolet A but not ultraviolet B radiation requires melanin pigment. *Nat Commun* **3**, 884 (2012).
36. Mouret, S.*, et al.* Cyclobutane pyrimidine dimers are predominant DNA lesions in whole human skin exposed to UVA radiation. *Proc Natl Acad Sci U S A* **103**, 13765-13770 (2006).
37. Mouret, S., Forestier, A. & Douki, T. The specificity of UVA-induced DNA damage in human melanocytes. *Photochem Photobiol Sci* **11**, 155-162 (2012).
38. Larsson, P., Andersson, E., Johansson, U., Ollinger, K. & Rosdahl, I. Ultraviolet A and B affect human melanocytes and keratinocytes differently. A study of oxidative alterations and apoptosis. *Exp Dermatol* **14**, 117-123 (2005).
39. de Leeuw, S.M.*, et al.* The UV action spectra for the clone-forming ability of cultured human melanocytes and keratinocytes. *Photochem Photobiol* **59**, 430-436 (1994).
40. Swope, V.B., Starner, R.J., Rauck, C. & Abdel-Malek, Z.A. Endothelin-1 and alpha-melanocortin have redundant effects on global genome repair in UV-irradiated human melanocytes despite distinct signaling pathways. *Pigment Cell Melanoma Res* (2019).
41. Ikehata, H., Kudo, H., Masuda, T. & Ono, T. UVA induces C-->T transitions at methyl-CpG-associated dipyrimidine sites in mouse skin epidermis more frequently than UVB. *Mutagenesis* **18**, 511-519 (2003).
42. Brash, D.E. UV signature mutations. *Photochem Photobiol* **91**, 15-26 (2015).
43. Cannistraro, V.J. & Taylor, J.S. Acceleration of 5-methylcytosine deamination in cyclobutane dimers by G and its implications for UV-induced C-to-T mutation hotspots. *J Mol Biol* **392**, 1145-1157 (2009).
44. Ikehata, H., Chang, Y., Yokoi, M., Yamamoto, M. & Hanaoka, F. Remarkable induction of UV-signature mutations at the 3'-cytosine of dipyrimidine sites except at 5'-TCG-3' in the UVB-

exposed skin epidermis of xeroderma pigmentosum variant model mice. *DNA Repair (Amst)* **22**, 112-122 (2014).
45. Cannistraro, V.J., Pondugula, S., Song, Q. & Taylor, J.S. Rapid deamination of cyclobutane pyrimidine dimer photoproducts at TCG sites in a translationally and rotationally positioned nucleosome in vivo. *J Biol Chem* **290**, 26597-26609 (2015).
46. Ikehata, H. Mechanistic considerations on the wavelength-dependent variations of UVR genotoxicity and mutagenesis in skin: the discrimination of UVA-signature from UV-signature mutation. *Photochem Photobiol Sci* **17**, 1861-1871 (2018).
47. Davies, H.*, et al.* Mutations of the BRAF gene in human cancer. *Nature* **417**, 949-954 (2002).
48. Robertson, A.G.*, et al.* Integrative Analysis Identifies Four Molecular and Clinical Subsets in Uveal Melanoma. *Cancer cell* **32**, 204-220 e215 (2017).
49. Shah, C.P., Weis, E., Lajous, M., Shields, J.A. & Shields, C.L. Intermittent and chronic ultraviolet light exposure and uveal melanoma: a meta-analysis. *Ophthalmology* **112**, 1599-1607 (2005).
50. Tenkate, T.D. Ocular ultraviolet radiation exposure of welders. *Scand J Work Environ Health* **43**, 287-288 (2017).
51. Tenkate, T.D. & Collins, M.J. Personal ultraviolet radiation exposure of workers in a welding environment. *Am Ind Hyg Assoc J* **58**, 33-38 (1997).
52. Hanawalt, P.C. & Spivak, G. Transcription-coupled DNA repair: two decades of progress and surprises. *Nat Rev Mol Cell Biol* **9**, 958-970 (2008).
53. Diffey, B.L. Sources and measurement of ultraviolet radiation. *Methods* **28**, 4-13 (2002).
54. Dowdy, J.C.*, et al.* FDA-sunlamp recommended Maximum Timer Interval And Exposure Schedule: consensus ISO/CIE dose equivalence. *Health Phys* **101**, 227-232 (2011).
55. Banerjee, S.S. & Harris, M. Morphological and immunophenotypic variations in malignant melanoma. *Histopathology* **36**, 387-402 (2000).
56. Li, H. & Durbin, R. Fast and accurate short read alignment with Burrows-Wheeler transform. *Bioinformatics* **25**, 1754-1760 (2009).
57. Picard - A set of tools (in Java) for working with next-generation sequencing data in the BAM format.
58. McKenna, A.*, et al.* The Genome Analysis Toolkit: a MapReduce framework for analyzing next-generation DNA sequencing data. *Genome research* **20**, 1297-1303 (2010).
59. Koboldt, D.C.*, et al.* VarScan 2: somatic mutation and copy number alteration discovery in cancer by exome sequencing. *Genome research* **22**, 568-576 (2012).
60. McLaren, W.*, et al.* The Ensembl Variant Effect Predictor. *Genome Biol* **17**, 122 (2016).
61. Cerami, E.*, et al.* The cBio cancer genomics portal: an open platform for exploring multidimensional cancer genomics data. *Cancer discovery* **2**, 401-404 (2012).
62. Gu, Z., Eils, R. & Schlesner, M. Complex heatmaps reveal patterns and correlations in multidimensional genomic data. *Bioinformatics* **32**, 2847-2849 (2016).
63. Kramer, A., Green, J., Pollard, J., Jr. & Tugendreich, S. Causal analysis approaches in Ingenuity Pathway Analysis. *Bioinformatics* **30**, 523-530 (2014).
64. Talevich, E., Shain, A.H., Botton, T. & Bastian, B.C. CNVkit: Genome-Wide Copy Number Detection and Visualization from Targeted DNA Sequencing. *PLoS computational biology* **12**, e1004873 (2016).
65. Blokzijl, F., Janssen, R., van Boxtel, R. & Cuppen, E. MutationalPatterns: comprehensive genome-wide analysis of mutational processes. *Genome Med* **10**, 33 (2018).

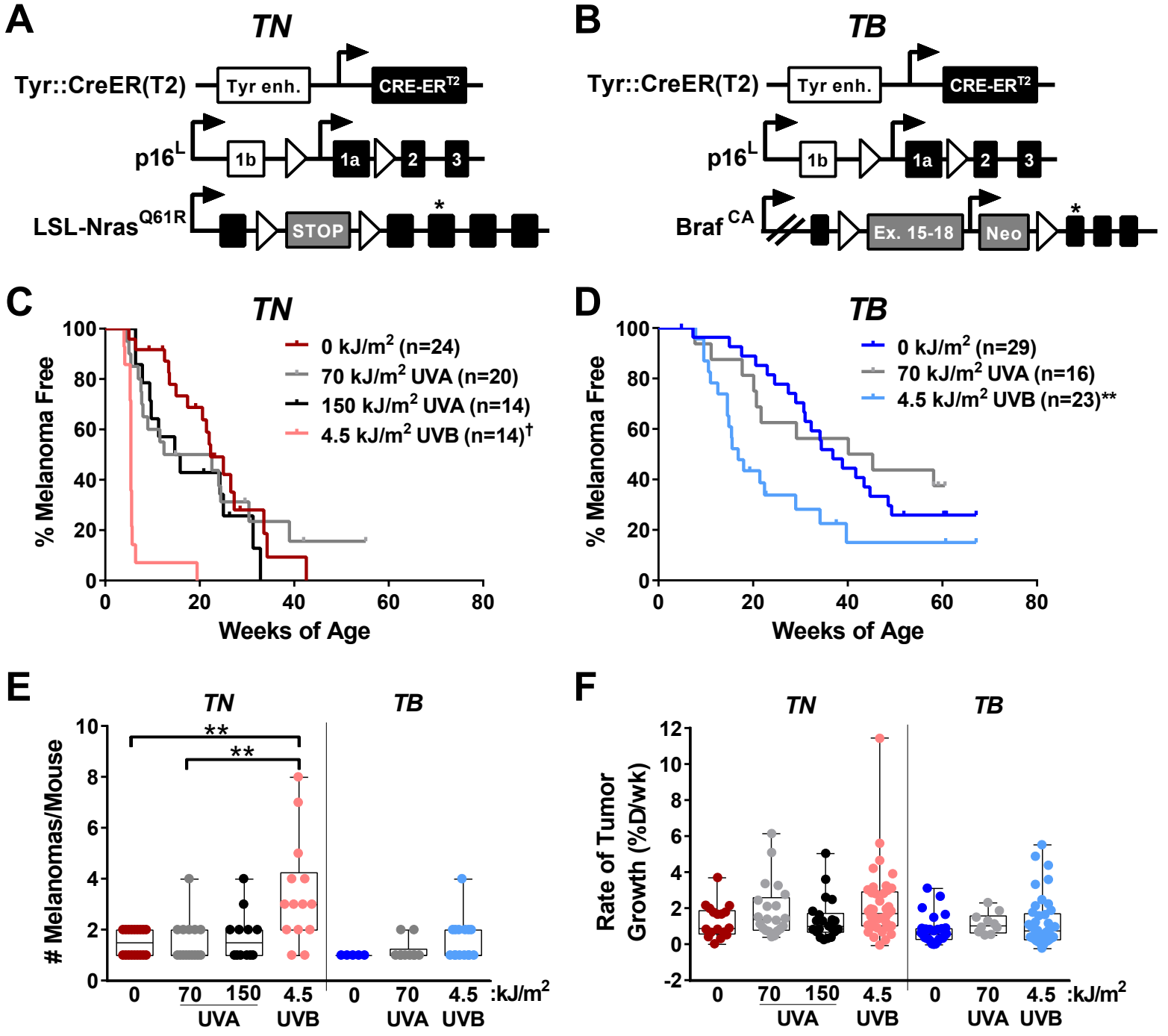
A
TN
Tyr::CreER(T2)
Tyr enh.
CRE-ERT2
p16L
1b
1a
2
3
LSL-NrasQ61R
STOP
*
B
TB
Tyr::CreER(T2)
Tyr enh.
CRE-ERT2
p16L
1b
1a
2
3
Braf CA
Ex. 15-18
Neo
*
C
TN
% Melanoma Free
Weeks of Age
0 kJ/m2 (n=24)
70 kJ/m2 UVA (n=20)
150 kJ/m2 UVA (n=14)
4.5 kJ/m2 UVB (n=14)†
D
TB
% Melanoma Free
Weeks of Age
0 kJ/m2 (n=29)
70 kJ/m2 UVA (n=16)
4.5 kJ/m2 UVB (n=23)**
E
TN
TB
Melanomas/Mouse
**
**
0
70
150
4.5
UVA
UVB
0
70
4.5
UVA
UVB
:kJ/m2
F
TN
TB
Rate of Tumor Growth (%D/wk)
0
70
150
4.5
UVA
UVB
0
70
4.5
UVA
UVB
:kJ/m2

Figure 1

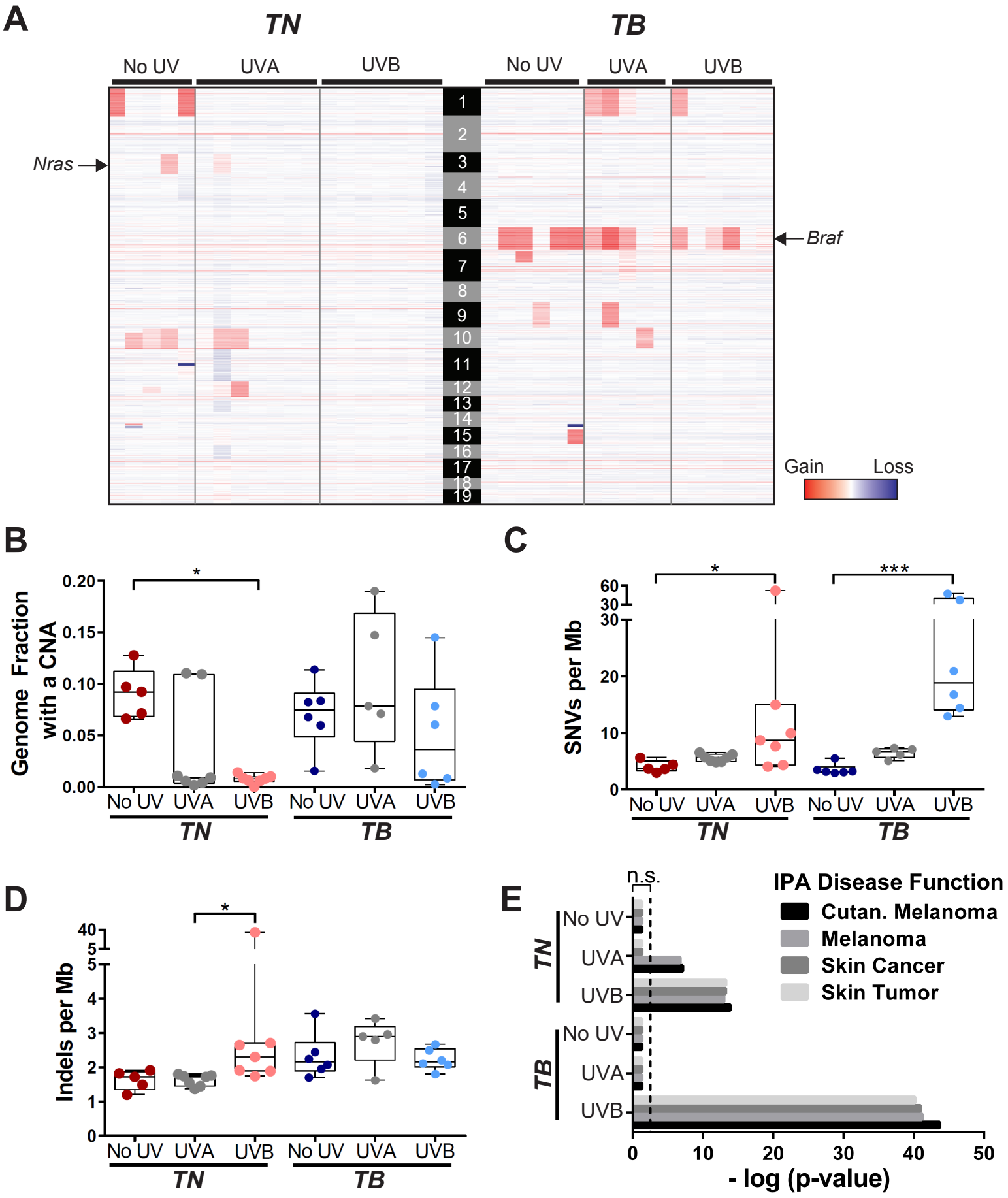
A
TN
TB
No UV
UVA
UVB
No UV
UVA
UVB
Nras
Braf
1
2
3
4
5
6
7
8
9
10
11
12
13
14
15
16
17
18
19
Gain
Loss
B
Genome Fraction with a CNA
0.20
0.15
0.10
0.05
0.00
*
No UV
UVA
UVB
No UV
UVA
UVB
TN
TB
C
SNVs per Mb
60
30
30
20
10
0
*
***
No UV
UVA
UVB
No UV
UVA
UVB
TN
TB
D
Indels per Mb
40
5
5
4
3
2
1
0
*
No UV
UVA
UVB
No UV
UVA
UVB
TN
TB
E
n.s.
IPA Disease Function
Cutan. Melanoma
Melanoma
Skin Cancer
Skin Tumor
TN
No UV
UVA
UVB
TB
No UV
UVA
UVB
0
10
20
30
40
50
- log (p-value)

Figure 2

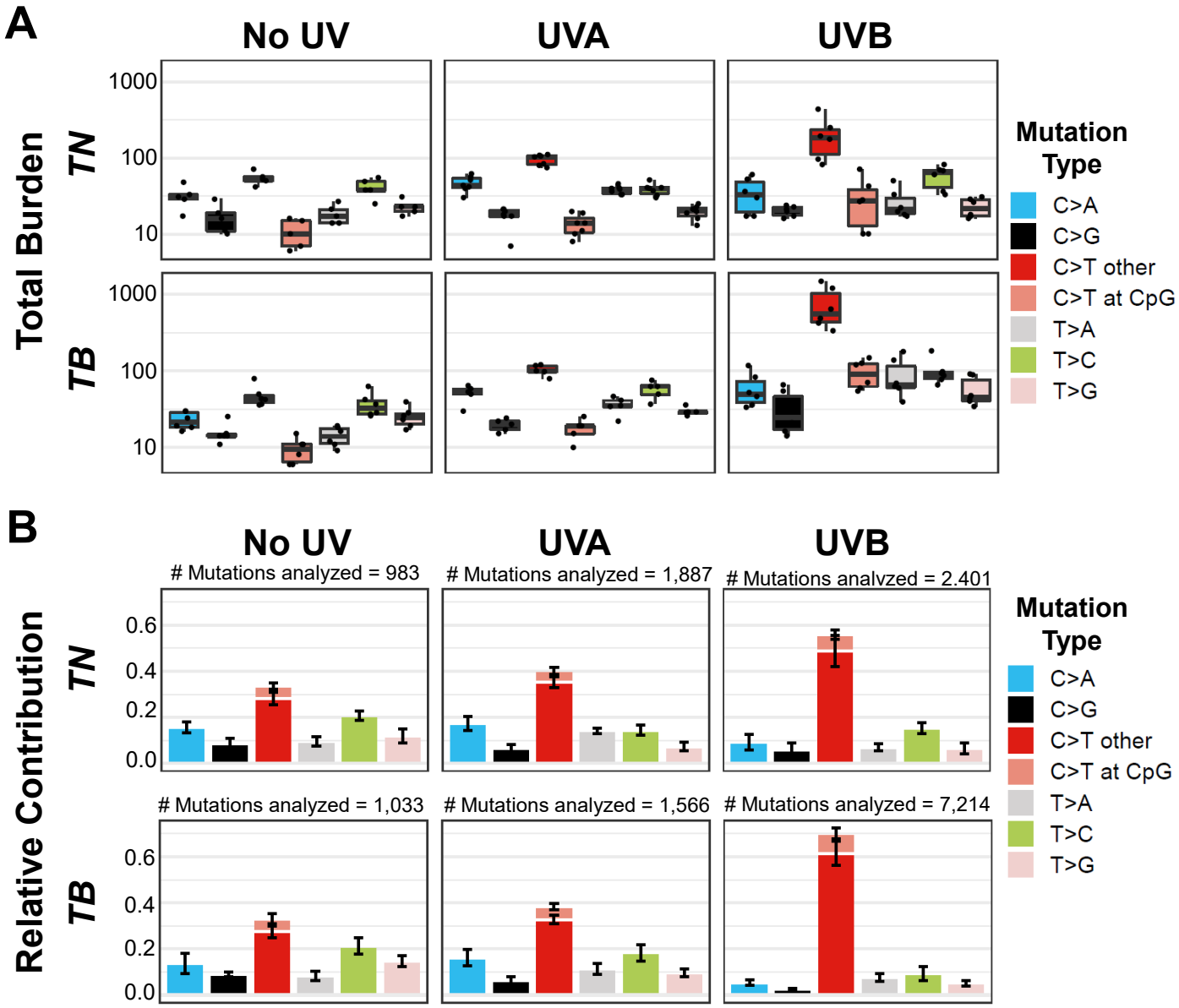
A
No UV
UVA
UVB
Total Burden
TN
TB
1000
100
10
Mutation Type
C>A
C>G
C>T other
C>T at CpG
T>A
T>C
T>G
B
No UV
UVA
UVB
Relative Contribution
Mutations analyzed = 983
Mutations analyzed = 1,887
Mutations analyzed = 2,401
Mutations analyzed = 1,033
Mutations analyzed = 1,566
Mutations analyzed = 7,214
0.6
0.4
0.2
0.0

Figure 3

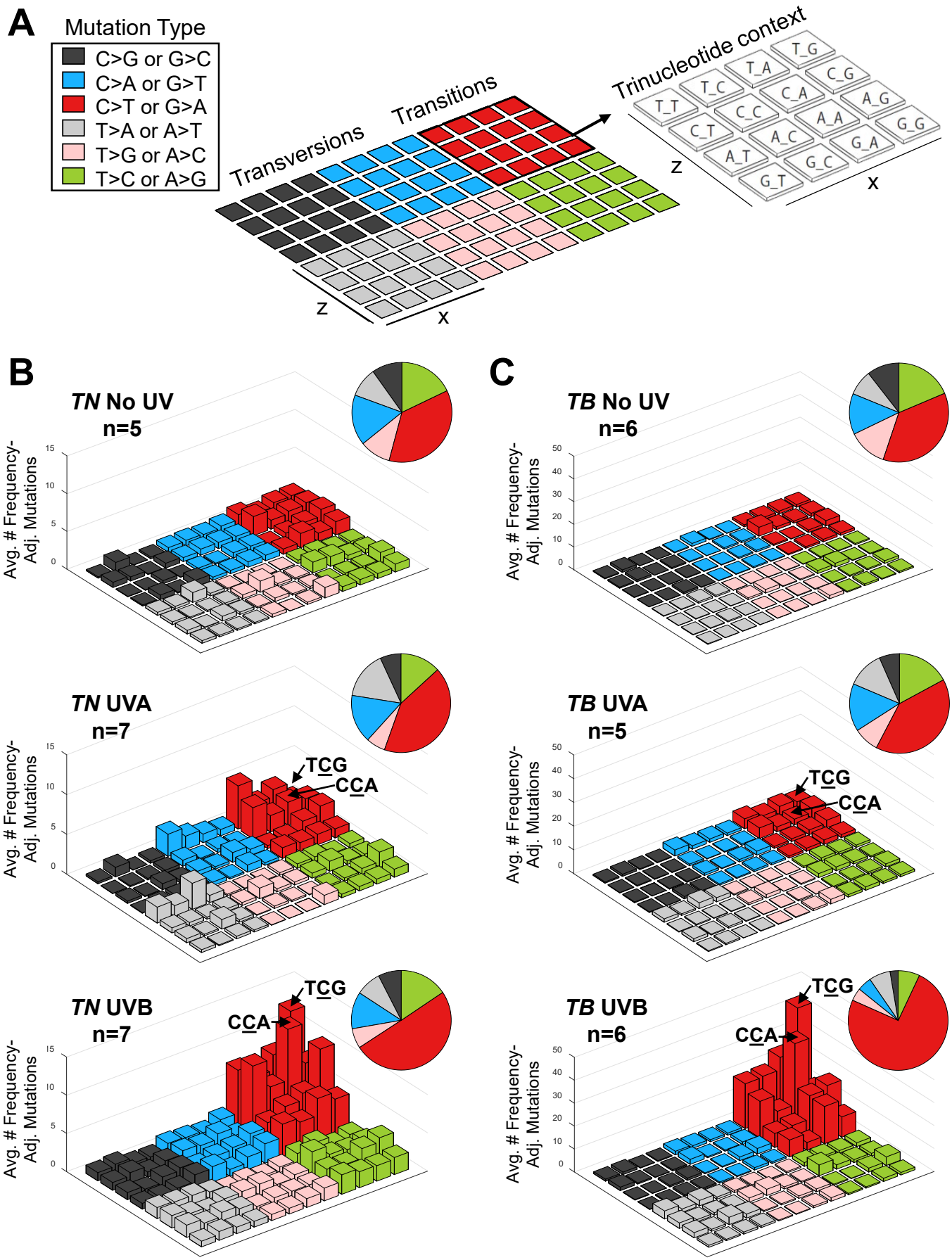
A
Mutation Type
C>G or G>C
C>A or G>T
C>T or G>A
T>A or A>T
T>G or A>C
T>C or A>G
Transversions
Transitions
Trinucleotide context
T_T
T_C
T_A
T_G
C_T
C_C
C_A
C_G
A_T
A_C
A_A
A_G
G_T
G_C
G_A
G_G
z
x
B
TN No UV
n=5
TN UVA
n=7
TCG
CCA
TN UVB
n=7
TCG
CCA
C
TB No UV
n=6
TB UVA
n=5
TCG
CCA
TB UVB
n=6
TCG
CCA
Avg. # Frequency-Adj. Mutations

Figure 4

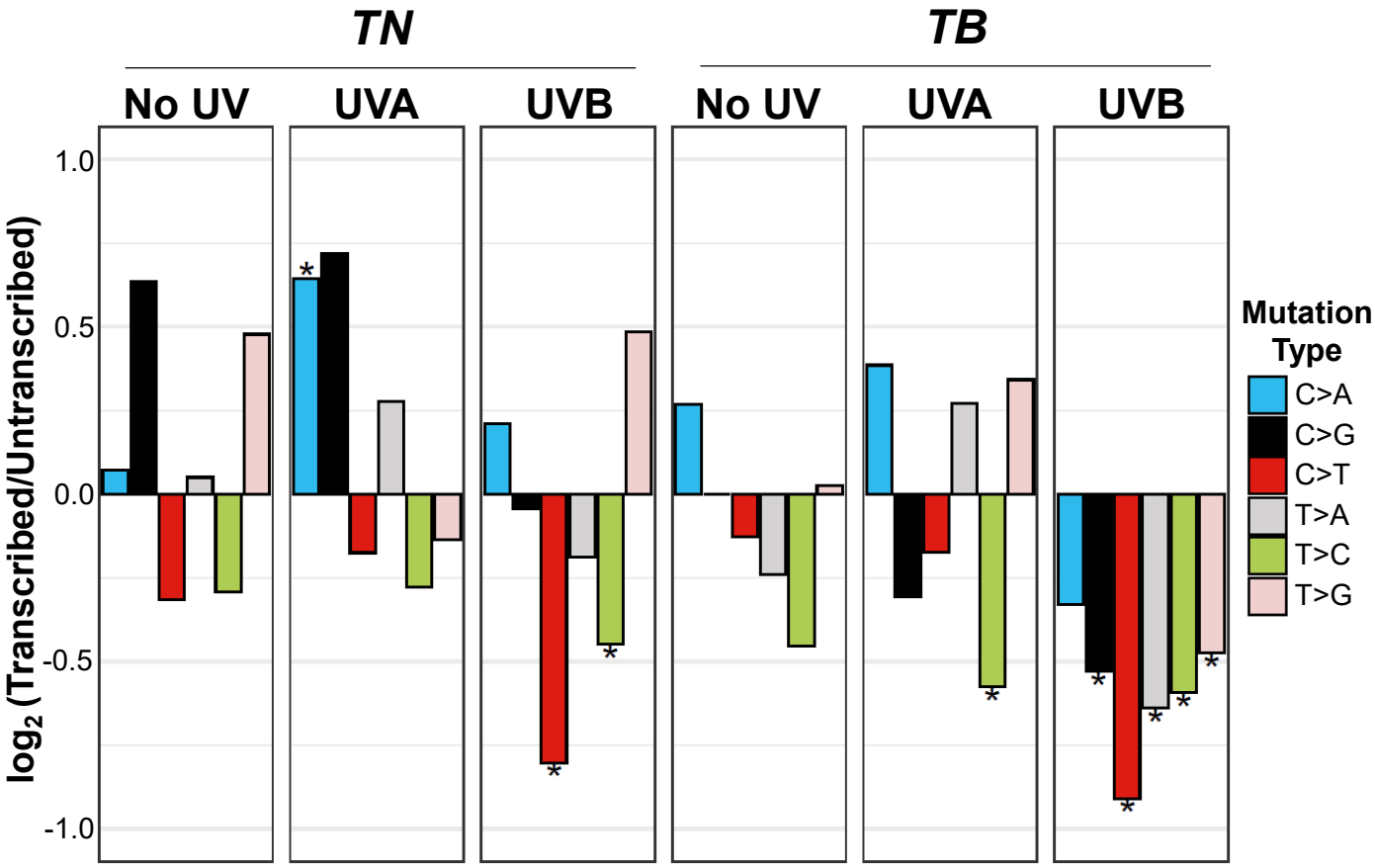
TN
TB
No UV
UVA
UVB
No UV
UVA
UVB
1.0
0.5
0.0
-0.5
-1.0
log2 (Transcribed/Untranscribed)
Mutation Type
C>A
C>G
C>T
T>A
T>C
T>G

Figure 5

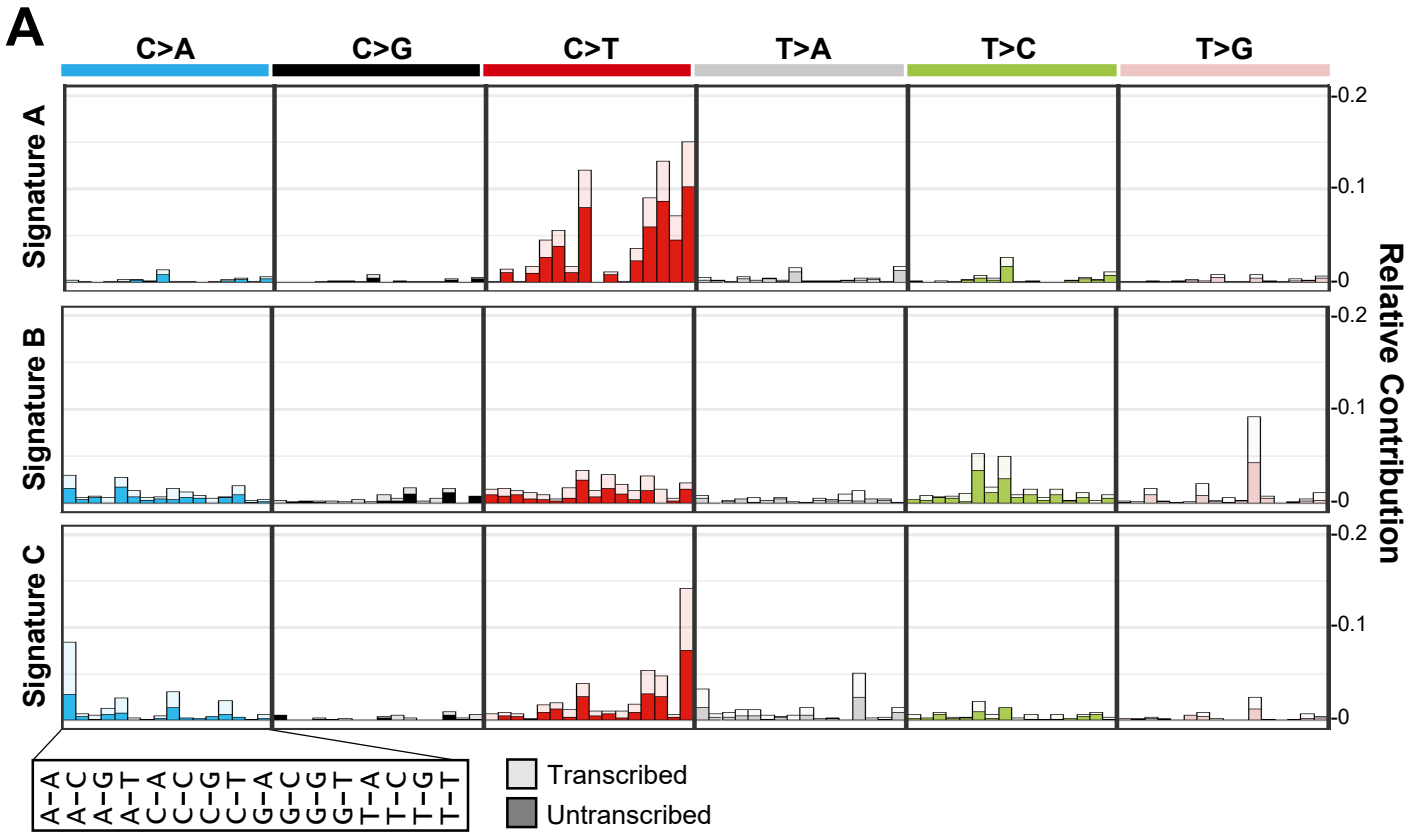
A
C>A
C>G
C>T
T>A
T>C
T>G
Signature A
Signature B
Signature C
Relative Contribution
0.2
0.1
0
A-A
A-C
A-G
A-T
C-A
C-C
C-G
C-T
G-A
G-C
G-G
G-T
T-A
T-C
T-G
T-T
Transcribed
Untranscribed

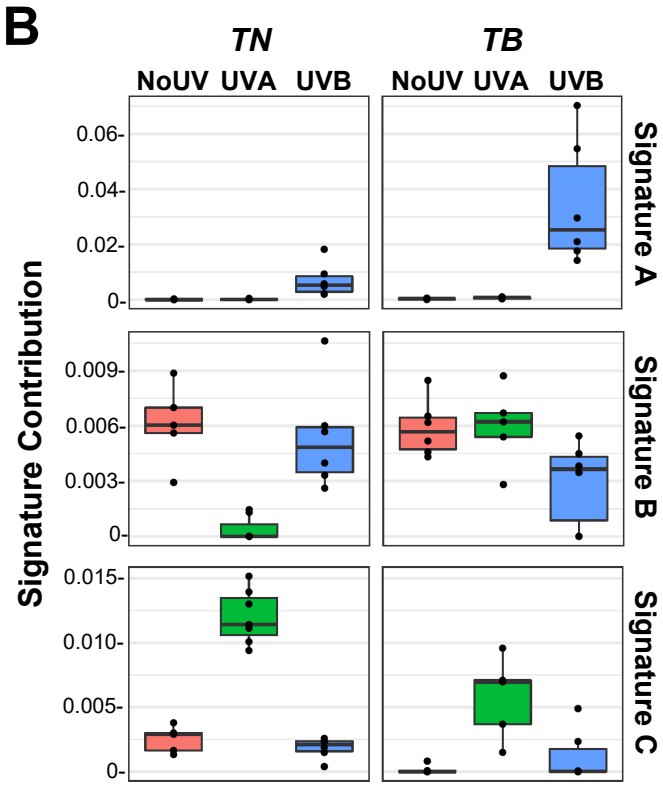
B
TN
TB
NoUV
UVA
UVB
Signature Contribution
Signature A
Signature B
Signature C
0.06
0.04
0.02
0
0.009
0.006
0.003
0.015
0.010
0.005

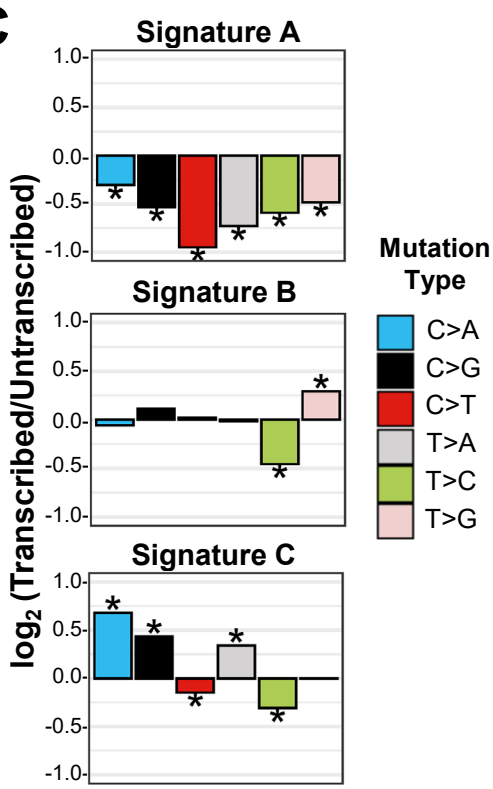
C
Signature A
Signature B
Signature C
log2 (Transcribed/Untranscribed)
1.0
0.5
0.0
-0.5
-1.0
Mutation Type
C>A
C>G
C>T
T>A
T>C
T>G

Figure 6

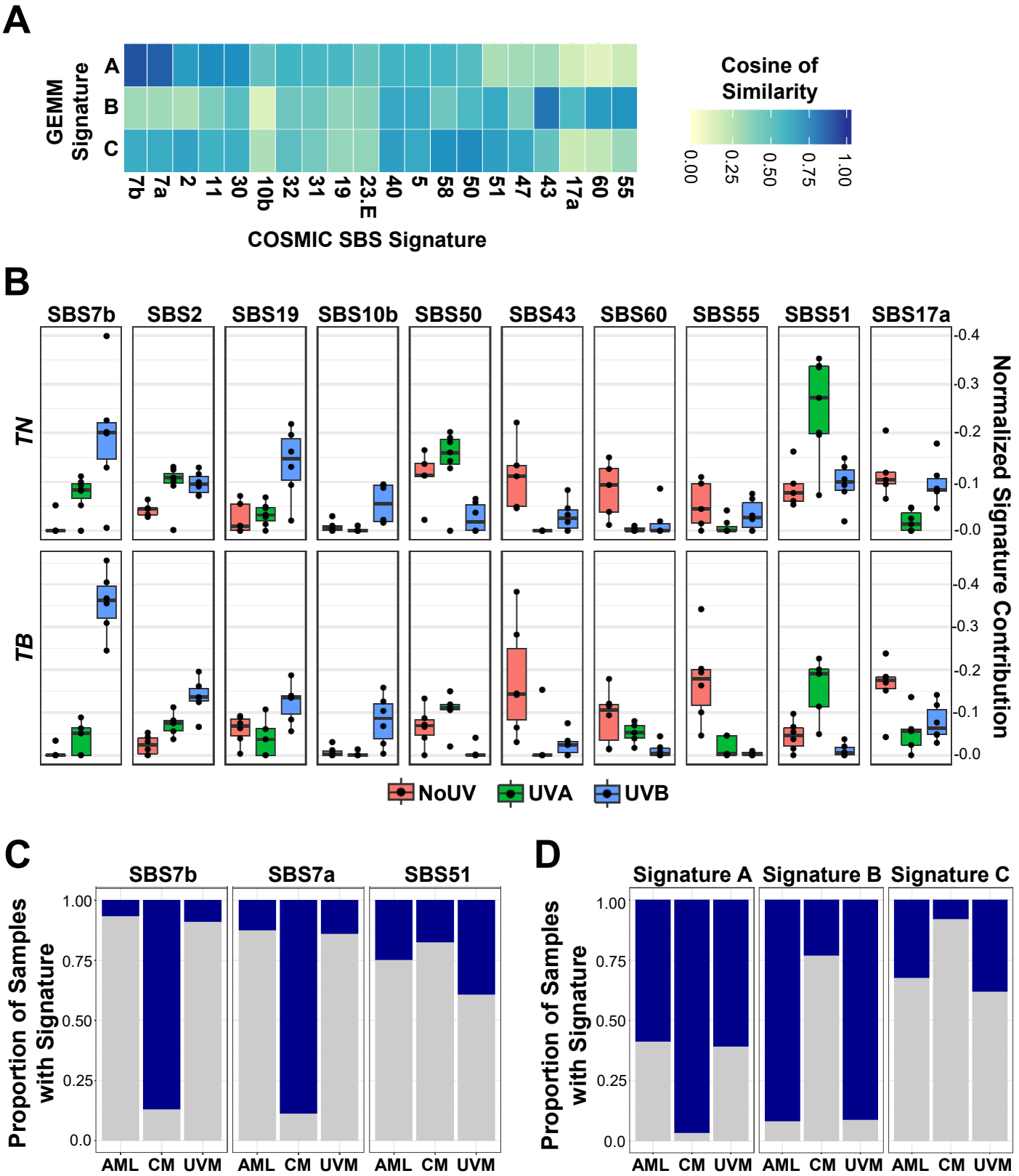
A
GEMM Signature
A
B
C
7b
7a
2
11
30
10b
32
31
19
23.E
40
5
58
50
51
47
43
17a
60
55
COSMIC SBS Signature
Cosine of Similarity
0.00
0.25
0.50
0.75
1.00
B
SBS7b
SBS2
SBS19
SBS10b
SBS50
SBS43
SBS60
SBS55
SBS51
SBS17a
TN
TB
Normalized Signature Contribution
-0.4
-0.3
-0.2
-0.1
-0.0
NoUV
UVA
UVB
C
SBS7b
SBS7a
SBS51
Proportion of Samples with Signature
1.00
0.75
0.50
0.25
0.0
AML
CM
UVM
D
Signature A
Signature B
Signature C

Figure 7

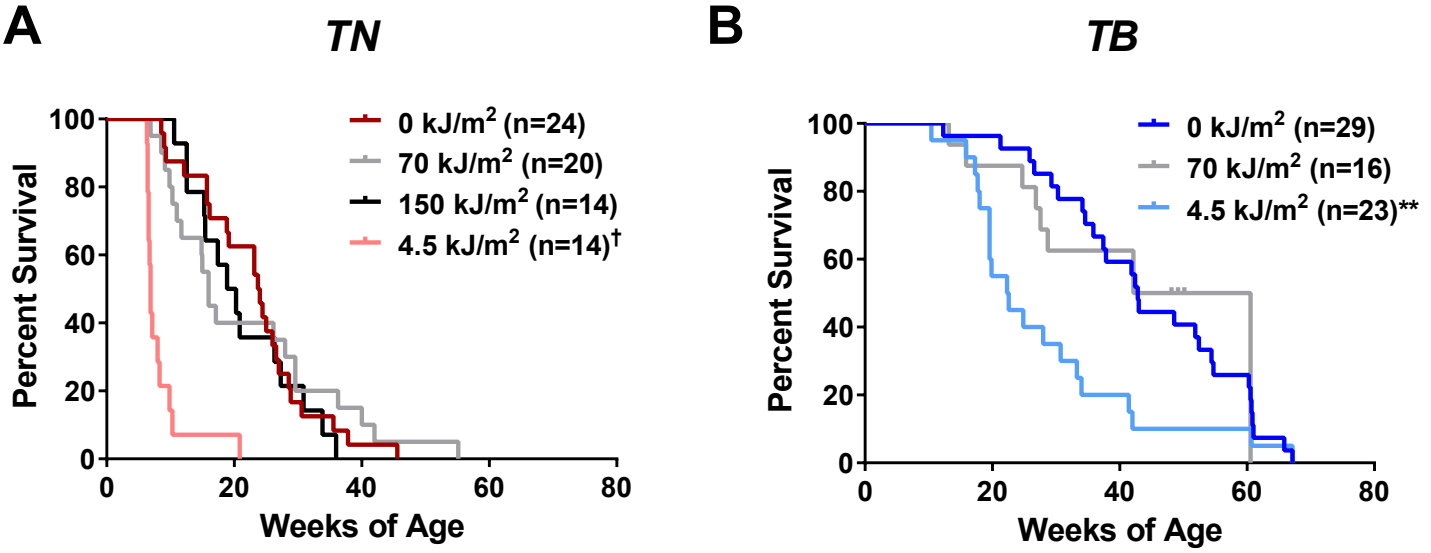
A
TN
Percent Survival
Weeks of Age
0 kJ/m2 (n=24)
70 kJ/m2 (n=20)
150 kJ/m2 (n=14)
4.5 kJ/m2 (n=14)†
B
TB
Percent Survival
Weeks of Age
0 kJ/m2 (n=29)
70 kJ/m2 (n=16)
4.5 kJ/m2 (n=23)**

Figure S1

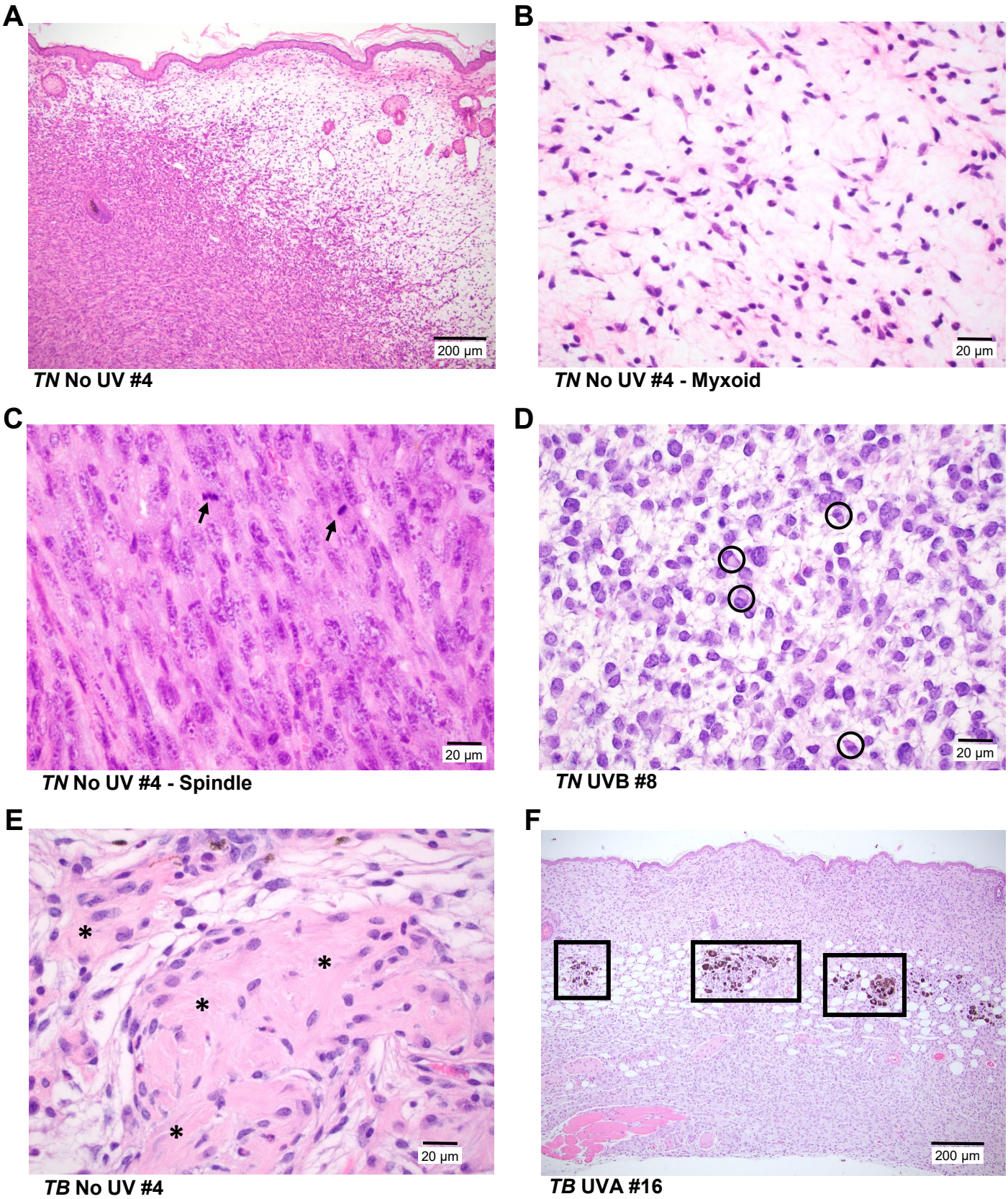
A
200 µm
TN No UV #4
B
20 µm
TN No UV #4 - Myxoid
C
20 µm
TN No UV #4 - Spindle
D
20 µm
TN UVB #8
E
20 µm
TB No UV #4
F
200 µm
TB UVA #16

Figure S2

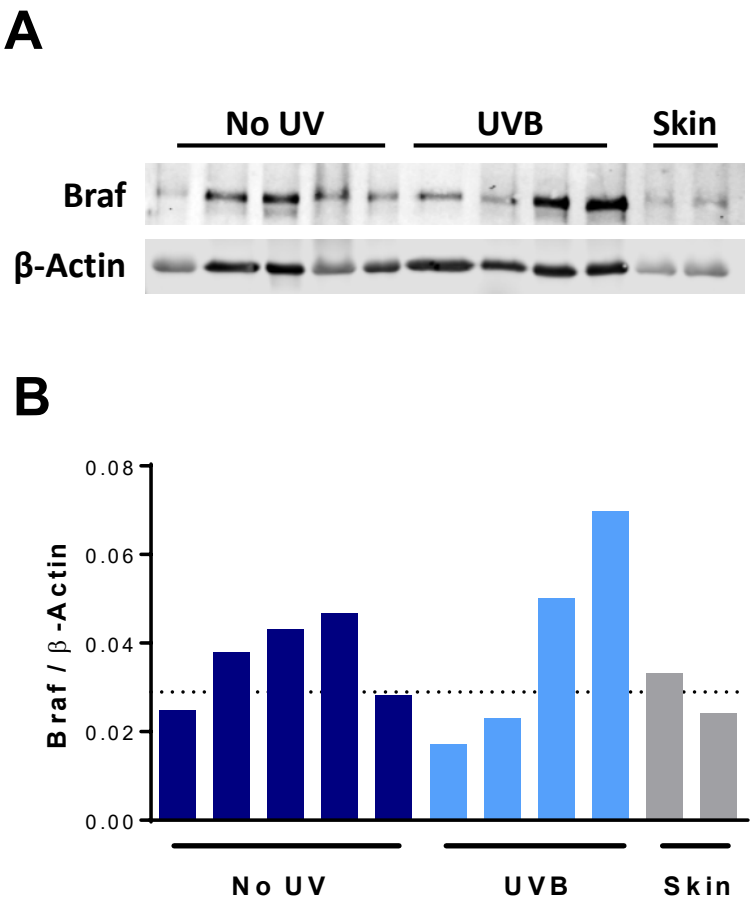
A
No UV
UVB
Skin
Braf
β-Actin
B
0.08
0.06
0.04
0.02
0.00
Braf / β-Actin
No UV
UVB
Skin

Figure S3

Mutations overlapping with human melanoma
80
60
40
20
0
Samples with each gene mutation
0
2
4
Alterations
indel
frameshift
missense
splicevar
startstop
No UV
UVA
UVB
No UV
UVA
UVB
TpN
TpB

Figure S4